Chemical Engineering Journal 485 (2024) 149894

Contents lists available at ScienceDirect

Chemical Engineering Journal

journal homepage: www.elsevier.com/locate/cej

Ab initio modelling of photocatalytic CO_2 reduction reactions over Cu/TiO_2 semiconductors including the electronic excitation effects

Žan Kovačič [a], Blaž Likozar [a,*], Matej Huš [a,b,c,*]

[a] National Institute of Chemistry, Department of Catalysis and Chemical Reaction Engineering, Hajdrihova 19 SI-1000 Ljubljana, Slovenia
[b] Association for Technical Culture of Slovenia (ZOTKS), Zaloška 65 SI-1000 Ljubljana, Slovenia
[c] Institute for the Protection of Cultural Heritage of Slovenia (ZVKDS), Poljanska 40 SI-1000 Ljubljana, Slovenia

ARTICLE INFO

Keywords:
Density Functional Theory (DFT)
Excited states
CO_2 photoreduction
Photocatalysis
Microkinetic model

ABSTRACT

Photocatalysis is a promising method for reducing CO_2 in an environmentally friendly way. Despite extensive experimental studies, theoretical studies lag behind and often resort to describing catalysts in the excited state, while the reaction mechanism is mostly studied at the ground level. We theoretically calculate a full reaction mechanism of CO_2 reduction to CO in the excited state for five surfaces: Cu(1 1 1), anatase(1 1 0), rutile(1 0 1) and Cu/anatase, Cu/rutile using the ΔSCF approach. We show that excited states considerably lower activation barriers, making it necessary in describing the experimental performance. The density functional theory calculations in the excited state are used to construct a microkinetic model, which is used to predict the performance of each catalytic surface. We show that Cu(1 1 1) is photocatalytically inactive, TiO_2 is only active in the UV range and catalyzes water splitting. Only Cu/rutile is active for CO_2 reduction to CO, while Cu/anatase produces more H_2.

1. Introduction

Titanium dioxide (TiO_2) is one of the most studied semiconductor materials, both experimentally and theoretically, on account of its photoactivity and a range of other potential applications [1]. Recently, its utilization in the field of photocatalysis has become increasingly important as it represents a way to carry out catalytic reactions with lower energy consumption. TiO_2 can be found in several crystal phases, which differ in their photocatalytic activity. Rutile and anatase are the most alluring phases, while occasionally brookite is also studied [2,3]. Nevertheless, pristine anatase and rutile TiO_2 have some drawbacks, such as high band gaps (above 3 eV), which means that only UV light is able to excite the electrons from the valence band (VB) to the conduction band (CB). In order to boost the photoactivity in the visible light range, modifications which decrease the band gap (utilizing visible light) are required. Moreover, other adverse phenomena must also be suppressed, such as charge recombination [4,5], while charge transfer should be increased. There are several strategies to solve these problems: doping [6,7], the deposition of co-catalysts [8,9,10,11], the integration of defects (e.g. oxygen vacancies [12]) or using the so called Z-scheme photocatalyst [13,14].

Furthermore, in undoped TiO_2, electrons would sink into the bulk and recombine, which is a well-known deficiency of pristine TiO_2 [15]. Doping makes the material catalytically active by allowing electrons to reach the surface. In addition, metal doping controls the selectivity of the catalysts toward the desired products, which can range from CO and CH_3OH to higher hydrocarbons in the case of CO_2 photoreduction. Dopants can be considered defects and act in various roles. They can make the material more catalytically active by allowing the electrons to reach the surface. However, it can also create states that trap the charge carrier or act as recombination centers, hindering photocatalytic activity. Surface dopants often act as electron traps and boost the photoactivity [16], while bulk dopants act as recombination centers [12,17]. Furthermore, TiO_2 is frequently doped also to increase its absorption in the visible part of the spectrum.

Since experimental testing of all possible changes is unwieldy, *in-silico* calculations can be performed instead. Increasing computational power has led to an increase in theoretical studies of photocatalysis in recent years. However, the vast majority of theoretical studies focus either on the calculation of catalyst properties [18,19] or on phenomenological kinetic modelling of experimental results. When a reaction mechanism is studied *ab initio*, including all possible intermediates,

* Corresponding authors at: National Institute of Chemistry, Department of Catalysis and Chemical Reaction Engineering, Hajdrihova 19 SI-1000 Ljubljana, Slovenia (B. Likozar and M. Huš).
E-mail addresses: blaz.likozar@ki.si (B. Likozar), matej.hus@ki.si (M. Huš).

https://doi.org/10.1016/j.cej.2024.149894
Received 29 September 2023; Received in revised form 1 February 2024; Accepted 20 February 2024
Available online 23 February 2024
1385-8947/© 2024 The Author(s). Published by Elsevier B.V. This is an open access article under the CC BY-NC license (http://creativecommons.org/licenses/by-nc/4.0/).

activation barriers, and kinetic parameters, calculations are usually performed in the ground state [20,21]. However, the explicit consideration of the excited state is crucial for the correct representation of a photocatalytic process.

An alternative approach to modelling photocatalytic reactions uses the fact that the dielectric constant of TiO_2 is large enough to treat electrons and holes as free as opposed to excitons [22]. In this approximation, the mechanism can also be investigated using electro-chemical methods (grand canonical DFT or JDFT). In this work, however, we opted for the photochemistry approach.

Since there is a vast body of literature on CO_2 photoreduction, we shall focus on the studies closely related to this paper. Ji et al. [21] studied the reaction mechanism over defective (oxygen-vacant) and pristine anatase (1 0 1) TiO_2 in the ground state. Two mechanisms were proposed, namely fast hydrogenation and fast deoxygenation, where the first was found to be the dominant pathway according to DFT results. Another ground-state study investigated the reaction mechanism of CO_2 photoreduction towards methane over pristine and KBH doped g-C_3N_4 performed by Wang et al. [20]. Excited states are considered more rarely. Li et al. [23] studied the reaction mechanism over GaP (1 0 0)/TiO_2 (1 0 1) and accounted for the excitation by artificially increasing the H* surface coverage. On the other hand Ghuman et al. [24] studied the effects of excited states on the absorption spectra using the linear response time dependent density functional theory (LR-TDDFT). Le et al. [25] studied CO_2 dissociation over the Al@Cu_2O surface and explicitly incorporated the excited states in the reaction mechanism. The calculations were initially performed in the ground state, followed by a single point calculation of the excitation of the electron from the valence band to the conduction band using the ΔSCF method [26]. It was found that the effective energy barrier can be reduced by as much as 2 eV. Accounting for the excited states is therefore important to describe the true nature of a photocatalytic reaction mechanism.

The first excited is well described by a HOMO-LUMO transition for organic molecules. For metal centers, such an approach is admittedly less accurate TD-DFT and similar. However, a great advantage of the ΔSCF approach is its favorable computational cost. Often, this entirely precludes the use of TD-DFT for larger isolated or periodic system. In our work, ΔSCF had to be used due to relatively large unit cells of TiO_2. We investigated a simplified mechanism of CO_2 photoreduction on Cu (1 1 1), pristine anatase (1 0 1), pristine rutile (1 1 0) and Cu/rutile (1 1 0) and Cu/anatase (1 0 1) surface. First, ground-state calculations of the reaction mechanism are performed at the DFT level. Second, excited states are accounted for following Kasha's rule [27] by exciting one HOMO electron from the valence band to the LUMO orbital of the conduction band. The reaction mechanism and kinetics are then compared between different surfaces in the ground and excited state. Lastly, the results are benchmarked against existing literature data. The central focus of this study lies in the incorporation and significance of excited states, a novel approach that, to the best of our knowledge, has not been extensively explored by any other research group. Notably, this investigation covers a wide range of surfaces, adding to the complexity of the calculations involved. The innovative nature of this study stems from its comprehensive analysis of excited states on a larger scale, providing unique insights into their importance and implications.

2. Computational details

2.1. Ab initio calculations

Density functional theory (DFT) calculations were performed with the VASP-5.4.1 package [28]. The PBE functional in combination with the PAW pseudopotentials as implemented in the VASP package was employed [29,30]. The energy cut-off of 500 eV was shown to suffice for well converged results. To account for strong electron localization, the Hubbard correction [31] was applied. A value of $U - J = 4$ eV [32,33] was applied to the Ti *3d* electrons, following the approach by Dudarev [34]. Long range dispersion forces were considered with the D3 correction by Grimme [35]. Spin polarization was included for all the calculations.

To study surface phenomena, surface slabs were constructed as follows. For Cu (1 1 1), a 3-layer 6x6 supercell was prepared. A 3-layer 3x2 supercell of pristine anatase (1 0 1) and Cu/TiO_2 anatase (1 0 1) surface with one fixed layer, and a 3-layer 3x3 supercell of pristine rutile (1 1 0) and Cu/rutile (1 1 0) with two fixed layers were constructed. In all instances, 12 Å vacuum was added to the slabs to avoid spurious inter-cell interactions. A dipole correction [36] was applied in the z-direction. The supercells were sampled with a Monkhorst-Pack mesh [37], at 1x1x1 (Gamma point) due to the size of the supercells. A cluster of four pre-optimized Cu atoms was deposited and allowed to relax on pristine anatase (1 0 1) and rutile (1 1 0) surfaces. All structures were relaxed until the atomic force dropped below 0.05 eV/Å. The nudged elastic band in conjunction with the climbing image [38] was used to identify the transition states, which were refined with the dimer method [39].

Adsorption energy was calculated as:

$$E_{ads} = E_{species+surface} - E_{surface} - E_{species} \quad (1)$$

where $E_{species+surface}$ denotes the energy of the adsorbed species on the surface, $E_{surface}$ is the energy of a relaxed slab and $E_{species}$ is the energy of the species in the gas phase. The activation energy was calculated as:

$$E_A = E_{TS} - E_{R,} \quad (2)$$

where E_{TS} is the energy of transition state and E_R is the energy of the initial state. Finally, the reaction energy was calculated as:

$$\Delta E = E_P - E_R \quad (3)$$

where E_P is the energy of the final state. Zero-point energies were not calculated because the ΔSCF structures were not geometrically reoptimized.

For the excited-state calculations, we applied the delta self-consistent field (ΔSCF) [26] approach. Firstly the structures of the initial, final and transition states were optimized in the ground state. Subsequently, the density of states was analyzed for each structure to identify the orbital for electron insertion. Then, an electron was moved from the valence band maxima (VBM) into the conduction band minima (CBM), leaving a hole in the VBM. A triplet spin state was used to force the population of the LUMO and depopulation of HOMO. After the change in orbital population, orbitals are reoptimized, and the energy is computed from these orbital.

The ΔSCF approach was chosen due to a much lower computational cost than TDDFT. They were benchmarked on a smaller system and the discrepancy in the reported activation barriers for the first step in the hydrogenation of CO2 was less than 10 %. On the larger system, which is used in this work, the memory requirements of the TD-DFT approach were prohibitive.

2.2. Microkinetic model

To evaluate the time evolution of the heterogeneous photocatalytic process, we created a microkinetic model using DFT-calculated reaction parameters. The model assumes an ideal batch reactor with the following: constant temperature and pressure, no mass transfer limitations, ideal mixing, no lateral interactions. Since the microkinetic model was set up to compare the *differences* in reaction kinetics in the photo-activated and dark regime, the exact reactor parameters was less of a concern. Also, no attempt was made to describe the photoactivation process itself as this has been extensively studied before. Instead, we focused on the kinetics of the reaction once it is photoactivated.

To mathematically describe the transformation, we constructed and solved a system of differential equations for the gas and surface reactions along with a balance for the active sites. For the studied network, a

general differential equation for species i is written as:

$$\frac{dCi}{dt} = r_i^{ads} - r_i^{des} + \sum r_{i,n} \tag{4}$$

The symbol C_i represents bulk concentration, and r's refer to the reaction rates of adsorption, desorption, and elementary steps on the surface. The model assumes the Langmuir-Hinshelwood reaction mechanism [40], where two molecules adsorbed on neighboring surface sites undergo a bimolecular reaction. Diffusion is accounted for implicitly since the model does not distinguish individual sites and instead deals with average surface coverages.

The following elementary reaction steps are included in the micro-kinetic model, totaling 4 adsorption and 7 surface reactions.

$$H_2 + * \underset{kH_2rev}{\overset{kH_2}{\longleftrightarrow}} H_2^* \tag{5}$$

$$CO_2 + * \underset{kCO_2rev}{\overset{kCO_2}{\longleftrightarrow}} CO_2^* \tag{6}$$

$$CO + \ ^* \underset{kCOrev}{\overset{kCO}{\longleftrightarrow}} CO^* \tag{7}$$

$$H_2O + \ ^* \underset{kH_2Orev}{\overset{kH_2O}{\longleftrightarrow}} H_2O^* \tag{8}$$

$$H_2^* + \ ^* \underset{k_{-1}}{\overset{k_1}{\leftrightarrow}} 2H^* \tag{9}$$

$$CO_2^* + \ ^* \underset{k_{-2}}{\overset{k_2}{\leftrightarrow}} CO^* + O^* \tag{10}$$

$$O^* + H^* \underset{k_{-3}}{\overset{k_3}{\leftrightarrow}} OH^* + \ ^* \tag{11}$$

$$CO_2^* + H^* \underset{k_{-4}}{\overset{k_4}{\leftrightarrow}} c-COOH^* + \ ^* \tag{12}$$

$$t-COOH^* + * \underset{k_{-5}}{\overset{k_5}{\longleftrightarrow}} CO^* + OH^* \tag{13}$$

$$OH^* + H^* \underset{k_{-6}}{\overset{k_6}{\longleftrightarrow}} H_2O^* + * \tag{14}$$

$$c-COOH^* \underset{k_{-7}}{\overset{k_7}{\longleftrightarrow}} t-COOH^* \tag{15}$$

Asterisk denotes active surface site. We considered all reactions to be reversible and first order. The system of differential equations was solved with the SciPy package in Python. Given the complexity of the system, which encompasses vastly different reaction rates, we employed the LSODA solver, which switches between stiff and non-stiff methods. For the adsorption of gaseous species, the rate equation is expressed as:

$$r_{ads}^X = k_{ads}^X \theta_{empty} p_X, \tag{16}$$

where X is the studied species, p_X is the partial pressure, θ_{empty} is the empty active site and k_{ads}^X is the forward rate coefficient. For desorption, the rate is defined as:

$$r_{des}^X = k_{des}^X \theta_X \tag{17}$$

where k_{des}^X is the backward rate coefficient and θ_X is the surface coverage of species X. The forward reaction coefficient of non-activated adsorption can be approximated as:

$$k_{ads}^X = \frac{PA}{\sqrt{2\pi m^X k_B T}} \tag{18}$$

where P is the pressure (assumed 1 bar), A is the surface area of the active site (assumed approx. 0.1 nm^2 for TiO_2 [41]), m^X is the mass of the molecule and k_B is the Boltzmann constant [41]. For desorption, the pre-exponential and hence the rate is approximated as:

$$k_{des}^X = \frac{k_B T}{h} e^{\frac{E_{ads,X}}{k_B T}} \tag{19}$$

Here, h represents Planck's constant, and $E_{ads,X}$ denotes the adsorption energy, which is by definition negative. Furthermore, we disregarded the contribution of the translational, rotational, and vibrational degrees of freedom to the partition function.

For surface reactions, the reaction rates are calculated as:

$$k_{for} = \frac{k_B T}{h} e^{-\frac{E_{for}}{k_B T}} \tag{20}$$

$$k_{rev} = \frac{k_B T}{h} e^{-\frac{E_{rev}}{k_B T}} \tag{21}$$

where E_{for} and E_{rev} are the activation barriers in the forward and backward direction respectively. These can be calculated as:

$$E_{for} = E_{transition} - E_{reactant} \tag{22}$$

and

$$E_{rev} = E_{transition} - E_{product} \tag{23}$$

where $E_{transition}$ is the energy of the saddle point and $E_{reactant}$ and $E_{product}$ are the energies of the initial and final states (corresponding to the reactants and products), respectively. We modeled the reaction at 25 °C in H_2O and a pressure of 1 bar, with variations in the CO_2 feed pressure.

3. Results and discussion

Initially, adsorption of key intermediates on all five studied surfaces was evaluated. Epitomized by the seminal Sabatier principle, a good catalyst must not bind the reactants nor products too strongly nor too weakly. It has been shown that the adsorption energies not only correlate with the activation barriers, as implied by the Sabatier principle, but can on their own influence the reaction rates [42]. From a technical standpoint, adsorption must be evaluated to be able to study the reaction mechanism (shown in Eqs. (9)–(15) including barriers and reaction energies.

3.1. Electronic effects

Intially, we analyse the electronic structure of titanium dioxide, as it plays a crucial role in the photocatalytic reduction process and, more importantly, to ascertain that our model successfully reproduces existing data. Anatase TiO_2 has an experimentally measured indirect experimental band gap of 3.2 eV [43], which is known to be severely underestimated by LDA and GGA functionals. [44] In Fig. 1, we show that an unmodified PBE estimates the band gap at 2.10 eV, which agrees with other studies at this level [45,46]. Mitigation is possible with a cheap Hubbard correction or more expensive hybrid functionals. In this work, however, we use the cheaper GGA approach with a Hubbard correction, as opposed to the computationally expensive hybrid functionals, as a proof of concept.

We shift our attention to the density of states (DOS) calculation for pristine anatase (1 0 1) and Cu doped anatase (1 0 1) surface. As evident from Fig. 2A, the valence band of pristine anatase (1 0 1) surface is mainly composed of O-*p* orbitals, whereas the conduction band consists predominantly from Ti-*d* orbitals (Fig. 2A). The effect of adding Cu atoms to the surface of anatase (1 0 1) is shown Fig. 2B. The band gap of the composite decreases, although this happens locally due to the interplay of Cu-*d* and Ti-*d* orbitals in the valence band (VB), which is shifted higher. Additionally, the conduction band (CB) is locally ever so slightly lowered. Additionally a mid-gap state is evident in the 1 eV region attributed to the Cu-*d* and Ti-*d* orbitals. This effectively lowers

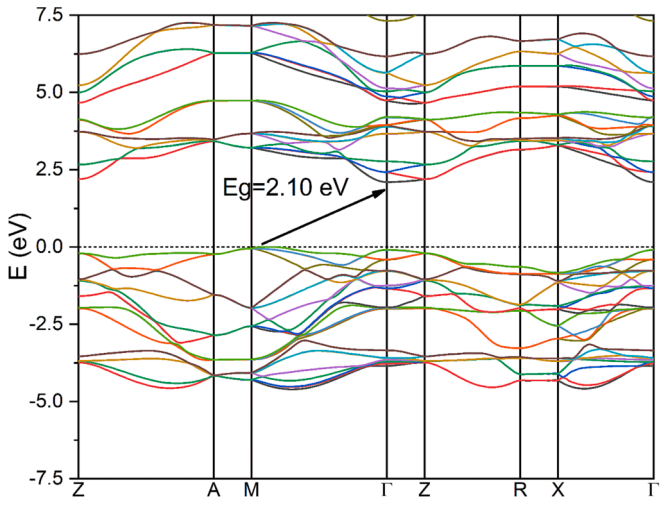

Fig. 1. Band structure of bulk anatase calculated with PBE. The Fermi energy is set at 0 eV.

the band gap locally (while the bulk band gap derived from TiO_2 remains unchanged, hence these states are localized at the surface) and can either act as a charge separator or recombination center. The observations regarding the mid-gap effects show some variation, with certain studies indicating a decrease in activity, while others point to an increase in photocatalytic activity. In Zhuang et al. [16] report, it was discovered that defects within the material's bulk serve as recombination centers, whereas surface defects like oxygen vacancies appear to enhance the photocatalytic activity [12]. This enhancement is attributed to their role as electron traps, which aligns with our own study, as metal deposits on surfaces act as electron sinks [47,48].

Lastly, we study the electronic effects of excitations. The charge density difference between the excited and ground state for Cu/anatase (1 0 1) with adsorbed CO and CO_2 is shown Fig. 3. Additionally, we show the integrated local density of states (ILDOS) for the valence band and the conduction band for both instances.

3.1.1. Cu (1 1 1)

First, copper was tested as a golden standard for CO_2 reduction and its (1 1 1) surface was chosen due to its thermodynamic stability. There has been ample research on this surface, for instance by Grabow et al. [49], which provided a benchmark for verifying our approach. Different adsorption sites were evaluated (fcc, hcp, bridge) and the most stable options are shown in Table 1.

Aside from HOCO, which is an unstable intermediate with an expectedly strong adsorption, only CO chemisorbs to the surface. CO_2, H_2 and H_2O merely physisorb, which is consistent with the findings from Grabow et al. [49]. Small differences are attributed to different calculation parameters, such as the use of the long-range Grimme D3 dispersion correction, a choice of functional (PBE vs PW91), K-point sampling, energy cut-off etc.

Table 2 depicts the activation barriers and reaction energies for the elementary steps considered in this study. H_2 dissociation exhibits an activation barrier of 0.41 eV and is exothermic by −0.54 eV. In comparison, Grabow et al. considered the reaction as a one-step dissociative adsorption with an energy change of −0.29 eV. The direct dissociation of CO_2 to CO and O species has an activation barrier of 1.21 eV and is endothermic by 0.80 eV, while hydrogenation of CO_2 to *c*-HOCO has an energy barrier of 1.58 eV and is endothermic by 0.56 eV. The subsequent dissociation of *t*-HOCO towards CO and OH has a low activation barrier of 0.50 eV but a virtually unchanged total energy change. The dissociation of *t*-HOCO has a barrier of 0.23 eV and is exothermic with an energy change of −0.52 eV. Lastly, H_2O can dissociate to form OH and H with an activation barrier of 0.87 eV and reaction energy of −0.18 eV or *vice versa* since water serves as a proton source. Our results are comparable with the findings of Grabow et al. [49] with some discrepancies due to differences in the computational details.

The formation of *t*-HOCO most likely occurs after the dissociation of CO_2 and H_2O, respectively, when CO and OH react with an energy barrier of 0.75 eV. On the other hand, a direct hydrogenation of CO_2 to *c*-HOCO requires a much higher activation energy of 1.58 eV. Once formed, HOCO could further react to form more reduced products (e.g., methane, methanol) but this is beyond the scope of the present study, which deals with the photoreduction of CO_2 to CO. The initial, saddle, and final structures are shown in Fig. S3.

Lastly, we estimate the effect of electron excitations. Following Kasha's rule [27], only the first excited state was taken into account. Since Cu (1 1 1) is metallic, DFT confirmed that excited electrons cannot significantly affect the energetics of the reaction as the valence and conduction bands overlap. Nevertheless, light can excite plasmons and the electron-hole channel could potentially affect the energetics (the plasmon decay channel is via the d-electrons). For consistency with the TiO_2 excitations, which allows a direct comparability of the results, this was omitted as we are only interested in the trends due to electronic excitations from the Fermi energy. The calculated reaction parameters shown in Table 2 confirm this. We observe that the activation barriers do not change significantly upon (photo)excitation. This is caused by the metallic nature of the Cu (1 1 1) surface, allowing charges to freely move between the valence band and conduction band.

3.1.2. Anatase (1 0 1)

We chose to investigate the pristine anatase (1 0 1) surface due to its thermodynamic stability and photocatalytic activity [50]. In Table 3, the calculated adsorption energies of the participating species is compared with literature data.

Sorescu et al. [51] calculated the adsorption of CO_2 on anatase (1 0 1) surface and found that the strongest adsorption has the adsorption energy −0.48 eV, which is in excellent agreement with our result (-0.43 eV). In both cases, CO_2 is adsorbed in a linear configuration with only minor perturbations to the electron density and most interaction stemming from the long-range dispersion corrections. Wanbayor et al. [52] investigated the adsorption of CO on anatase (1 0 1) surface (for subsequent oxidation towards CO_2) and calculated the adsorption energy at −0.26 eV, which is identical to our results. However, most studies on anatase (1 0 1) encompass some sort of surface modification, such as deposition of co-catalysts [55], doping [56] or defects formation (e.g. oxygen vacancies [21]) to boost its photocatalytic activity, making comparisons to the pristine case difficult. HOCO and H_2O adsorb more strongly with energies of −0.99 and −0.98 eV, respectively. For comparison, Vittadini et al. [54] estimated the adsorption energy of H_2O as −0.74 eV, which can be contributed to neglecting long range dispersion forces. H_2 physisorbs weakly (-0.20 eV), which agrees with the results from Wang et al. [53] (-0.34 eV).

In Table 4, activation barriers and reaction energies for the reaction on the pristine anatase (1 0 1) surface are shown. Hydrogen dissociation has a relatively high barrier of 1.00 eV and is endothermic by 0.36 eV. While the decomposition of H_2O into OH + H is easily accessible with a barrier of 0.50 eV and slightly endothermic by 0.37 eV, further hydrogenation of CO_2 to HOCO exhibits a high activation energy of 2.58 eV and is endothermic by 1.74 eV. Direct dissociation of CO_2 is not feasible due to a large activation energy of 4.86 eV and endothermicity of 4.46 eV. Thus, while TiO_2 can be used for water splitting provided that the irradiation wavelength is in the UV range, it is inactive for CO_2 reduction. The optimized geometries of the initial, saddle-point, and final structures are shown in Fig. S4.

As TiO_2 is a semiconductor commonly used in photocatalysis, excited-state calculations were performed. The calculated band gap of pristine anatase (1 0 1) surface was 2.36 eV (corresponding to wavelength of 525 nm or green color in the visible spectrum), which is reasonably close to the experimentally determined value of 3.2 eV

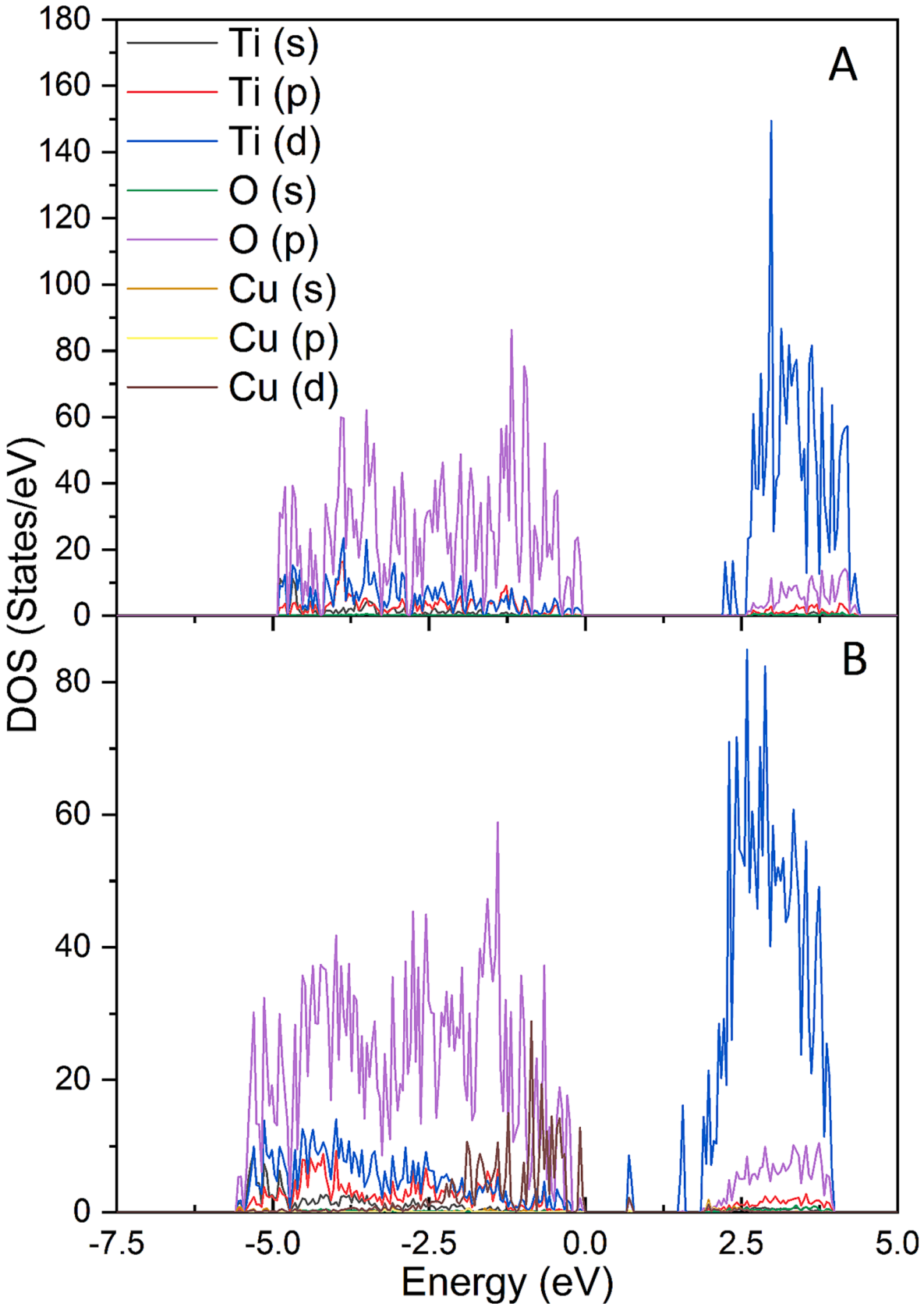

Fig. 2. Density of states (DOS) for A) Anatase (1 0 1) and B) Cu-anatase (1 0 1) surface. The Fermi energy is set at 0 eV.

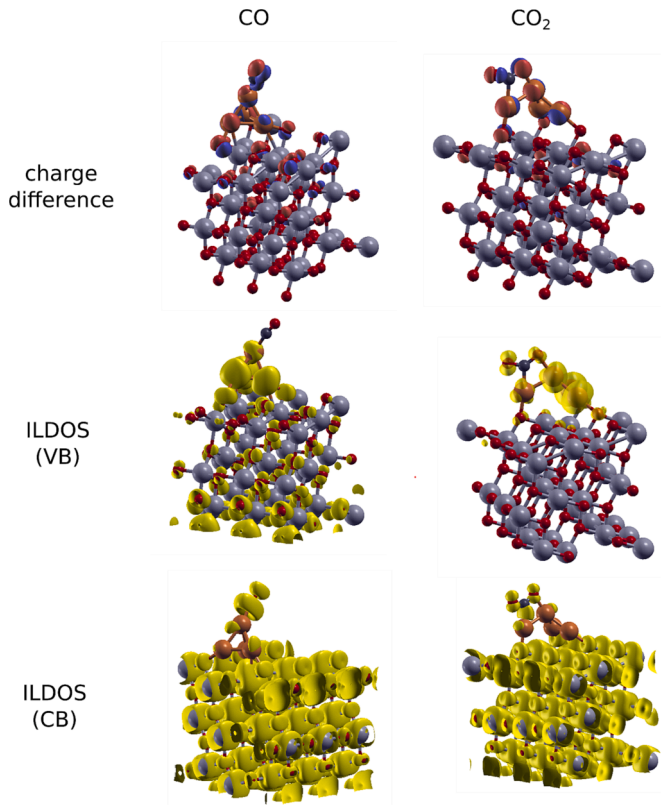

Fig. 3. (top) charge density difference between the ground and excited state, (middle) integrated local density of states (ILDOS) for the valence band, and (bottom) for the conduction band (CB). Left: CO, right: CO_2. Isovalue: 0.01 eV/Å^3.

Table 1
Adsorption energies [in eV] on the Cu (1 1 1) surface.

	This work	From Ref. [49]
CO_2	−0.22	−0.08
CO	−1.08	−0.86
c-HOCO	−2.24	−1.52
H_2	−0.07	n/a
H_2O	−0.17	−0.21

Table 2
Activation barriers and reaction energies [in eV] for the ground-state CO_2 reduction on the Cu (1 1 1) surface. Energies for the first excited state are given in brackets.

	E_A(this work)	ΔE(this work)	E_A Ref [49]	ΔE Ref [49]
$H_2 \rightarrow 2H$	0.41 (0.41)	−0.54 (-0.53)	n/a	−0.29
$CO_2 \rightarrow CO + O$	1.21 (1.21)	0.80 (0.81)	1.77	1.12
$CO_2 + H \rightarrow$ *c*-HOCO	1.58 (1.58)	0.56 (0.56)	1.78	0.55
t-HOCO$\rightarrow CO +$ *OH*	0.23 (0.23)	−0.52 (-0.54)	0.42	−0.14
$H_2O \rightarrow OH + H$	0.87 (0.87)	−0.18 (-0.18)	1.39	0.21
c-HOCO$\rightarrow$ *t*-HOCO	0.50 (0.50)	0.00 (0.00)	N/A	N/A

(corresponding to wavelength of 387 nm which under most definitions falls under the UV spectrum) [43]. The band gap is still underestimated due to well-known shortcomings of GGA functionals [57], although the Hubbard correction mitigated this effect to an extent, as previously discussed. In the excited state, H_2 dissociation is spontaneous and slightly exothermic at −0.17 eV. The activation energy for direct dissociation of CO_2 is lowered from 4.86 eV in the ground state to 2.74 eV in the excited state, which is still too high to expect any yields at ambient temperature and pressure. The hydrogenation of CO_2 to form HOCO also displays a high activation energy of 2.42 eV. Further dissociation of HOCO is also unfeasible due to even higher energy barriers, which are higher than > 3.5 eV and therefore inconsequential. Water dissociation has a barrier of 0.45 eV, which is similar to the ground state. The results suggest that although the inclusion of excited states has an effect on the reaction parameters it does not lower the barriers enough to make the CO_2 reduction feasible on the pristine anatase (1 0 1) surface.

Table 3
Adsorption energies [in eV] on the pristine anatase (1 0 1) surface.

	E_{ads}(this work)	E_{ads}(literature data)
CO_2	−0.43	−0.48 [51]
CO	−0.26	−0.26 [52]
c-HOCO	−0.99	n/a
H_2	−0.20	−0.34 [53]
H_2O	−0.98	−0.74 [54]

Table 4
Activation barriers and reaction energies [eV] for ground-state CO_2 reduction over pristine anatase (1 0 1) surface. Energies for the first excited state are given in brackets.

	E_A	ΔE
$H_2 \rightarrow 2H$	1.00 (0.00)	0.36 (-0.17)
$CO_2 \rightarrow CO + O$	4.86 (2.74)	4.46 (4.39)
$CO_2 + H \rightarrow$ *c-HOCO*	2.58 (2.42)	1.74 (2.42)
c-HOCO$\rightarrow CO + OH$	N/A	>3.5
$H_2O \rightarrow OH + H$	0.50 (0.00)	0.37 (0.33)

3.1.3. Rutile (1 1 0)

Rutile is the second crystal phase of titania that exhibits photocatalytic activity, and its (1 1 0) structure is not only the most thermodynamically stable but also the most extensively studied. In Table 5, adsorption energies of different intermediates are shown. CO_2 adsorbs with an energy of −0.47 eV, while Sorescu et al. reports an adsorption energy of −0.38 eV [58]. CO adsorbs much more weakly at −0.25 eV, which matches the results from Harris et al. [59]. This hints that the surface could be active for producing CO, which would easily desorb from the surface. H_2 exhibits a weak interaction with the surface at −0.19 eV, consistent with Lyalin et al. [60] reporting the adsorption energy similarly of −0.14 eV), whereas water adsorbs stronger at −1.27 eV (Harris et al. [59] report an identical value). Expectedly, HOCO exhibits a strong adsorption of −4.27 eV.

As shown in Table 6, the dissociation of H_2 has a low activation barrier of merely 0.26 eV and is also exothermic by −0.30 eV. Furthermore, H_2O dissociation is almost non-activated and exothermic (-0.24 eV), meaning that there should be ample supply of hydrogen on the catalytic surface. A direct dissociation of CO_2 is unfeasible due to a high reaction energy (>4 eV), similarly to the pristine anatase (1 0 1) surface. For direct CO_2 hydrogenation, the calculated activation barrier is 1.23 eV and is slightly exothermic (-0.19 eV). However, the subsequent dissociation of HOCO is thermodynamically prohibited due to a high reaction energy (>4 eV). This suggests that CO_2 reduction would only yield HOCO, which might react further to form other hydrocarbons

Table 5
Adsorption energies [in eV] on the pristine rutile (1 1 0) surface.

	E_{ads}	E_{ads}
CO_2	−0.47	−0.38 [58]
CO	−0.25	−0.25 [61]
c-HOCO	−4.27	n/a
H_2	−0.19	−0.14 [60]
H_2O	−1.27	−1.27 [59]

Table 6
Activation barriers and reaction energies [in eV] for CO_2 reduction over the pristine rutile (1 1 0) surface. Energies for the first excited state are given in brackets.

	E_A	ΔE
$H_2 \rightarrow 2H$	0.26 (0.00)	−0.30 (-0.34)
$CO_2 \rightarrow CO + O$	N/A	>3.5
$CO_2 + H \rightarrow$ *c-HOCO*	1.23 (1.09)	−0.19 (-0.11)
c-HOCO $\rightarrow CO + OH$	N/A	>3.5
$H_2O \rightarrow OH + H$	0.01 (0.00)	−0.24 (-0.26)

but this is out of scope of this study. For CO production, unmodified rutile is poorly suited. The initial, saddle-point and final structures are shown in Fig. S4.

We now focus on the excited-state effects in CO_2 reduction on a rutile (1 1 0) surface. H_2 dissociation is spontaneous and exothermic by −0.34 eV. While a direct dissociation of CO_2 is still prohibitively expensive and was thus not considered, we can assume that the barrier activation should be lower compared to ground state reaction, similar to anatase (1 0 1). The barrier for CO_2 hydrogenation is lowered from 1.23 eV in the ground state to 1.09 eV. However, its decomposition remains unfeasible due to high barriers. Water dissociation remains slightly exothermic with an energy change of –0.26 eV. As is the ground state, pure rutile is not suitable for CO_2 reduction. Provided the irradiation wavelength is suitable, water splitting is the predominant pathway. The calculated band gap of rutile (1 1 0) surface was 1.21 eV (which corresponds to wavelength of 1024 nm, falling in the domain of IR light), whereas the band gap of bulk rutile is 3.0 eV (corresponding to wavelength of 413 nm attributed to visible spectrum). The discrepancy is associated with the fact that band gaps of surfaces can differ from bulk quite significantly [62], additionally PBE functionals are known to underestimate band gaps, as mentioned before, although this is slightly remediated by introduction of Hubbard correction.

Comparing the results for unmodified, single-phase catalysts (Cu (1 1 1), anatase (1 0 1) and (1 1 0)) shows that they do not allow for CO_2 reduction or photoreduction. Since Cu (1 1 1) is metallic, exciting an electron from VBM to CBM has no impact on the energetics. With copper being one of the most active catalysts for CO_2 reduction, it would easily outperform anatase (1 0 1) or rutile (1 1 0). The latter show a considerable influence of photoexcitation on the activation barriers but would still fail to produce CO. On rutile (1 1 0), hydrogenation to HOCO would be preferred but it does not readily decompose into CO.

Thus, doped titania catalytic systems are inspected in the next section, where copper atoms have been deposited on its surface.

3.1.4. Cu/anatase (1 0 1)

Lastly, a two-phase Cu/TiO_2 catalyst surface was studied. Experimental research [63,64] has previously shown that Cu/TiO_2 catalysts combine the copper activity for CO_2 reduction and photoactivity of TiO_2. As described in Section 2, we placed four Cu atoms on the anatase (1 0 1) surface. First, several possible adsorption sites were probed with Cu_4 clusters (Fig. S1), where the one with the lowest energy was chosen for subsequent calculations. Depositing Cu on TiO_2 decreases the bandgap substantially and proportionally to the number of Cu atoms, which makes the photoactivation mechanism accessible below the UV light in the visible light spectrum. For instance, the calculated anatase (1 0 1) band gap is decreased from 2.36 eV (visible spectrum) to 0.35 eV (IR) upon depositing Cu_4. While this value is underestimated on the account of using PBE and the Hubbard correction, it still shows the general trend. Although this means that the photo-excited electron will have a lower energy relative to the pristine anatase (1 0 1) surface, this does not correlate simply with the catalytic activity of the surface as charge transfer, charge recombination, light absorption as well as surface-adsorbate interactions play a significant role.

Table 7 lists the adsorption energies of the intermediates involved in the reaction. CO_2 binds almost as weakly as on the pristine anatase surface (-0.37 vs. −0.43 eV respectively). In contrast, the adsorption of CO is much stronger on the Cu-decorated surface at −1.57 eV, which shows that CO can also react further once formed. HOCO also binds three times more strongly (-3.46 eV) than on pristine anatase. Furthermore, the Cu-decorated surface should be more saturated with H_2 due to the stronger binding, which is the typical spillover effect of Cu.

Table 7
Adsorption energies [in eV] on the Cu_4/anatase(1 0 1) surface.

	E_{ads}
CO_2	−0.37
CO	−1.57
t-HOCO	−3.46
H_2	−0.39
H_2O	−0.03

In Table 8, we observe that the activation energy needed to dissociate H_2 is higher (1.16 eV) than on pristine anatase 1.00 eV and slightly exothermic. However, more important is the low barrier for H_2O dissociation, which is only 0.14 eV and is exothermic by 1.46 eV. A direct dissociation of CO_2 has an activation energy of 1.66 eV and is exothermic by −0.67 eV, while it is endothermic on anatase (4.86 eV). Hydrogenation of CO_2 to form HOCO has a barrier of 1.71 eV (Fig. 4), which again outperforms pristine anatase (2.58 eV) and is only slightly higher than on the Cu (1 1 1) surface (1.58 eV). The same applies to the dissociation of HOCO. The initial, transition-state and final structures are shown in Fig. S5.

Lastly, we turn the attention to the inclusion of excited states. The dissociation activation energy of H_2 is 0.75 eV, which is significantly lower than in the ground state (1.16 eV). The barrier for H_2O dissociation is 0.01 eV and the reaction is more exothermic than in the ground state. The direct dissociation or hydrogenation of CO_2 is slightly more favorable in excited state than in ground state, which is attributed to the band structure of the catalyst. As the overlap of the orbitals is higher, resulting in lower band gaps, the photo-excited electrons in LUMO possess a lower energy relative to the ground state than in pristine anatase. Thus, the reaction pathway can follow either the dissociation or hydrogenation of CO_2 pathway due to comparable activation energy barriers, which is studied in the microkinetic model. While HOCO could react further to form methanol or methane, this is out of the scope of this paper, dealing with CO formation. However, due to its high adsorption energy (-1.57 eV) further reactions are possible.

3.1.5. Cu/Rutile(1 1 0)

A similar Cu_4/TiO_2 structure was also studied on the Cu/rutile (1 1 0) surface (Fig. S2). The adsorption energies over are presented in Table 9. CO_2 binds rather weakly to the surface at −0.28 eV, whereas CO exhibits a slightly stronger, yet still low interaction at −0.45 eV. HOCO adsorbs the strongest with −2.89 eV. On the other hand, H_2 and H_2O physisorb with adsorption energies −0.21 and −0.13 eV respectively. The relatively low adsorption energy of CO hints that it can be the major product.

Table 8
Activation barriers and reaction energies [in eV] for ground-state CO_2 reduction over Cu_4-anatase (1 0 1) surface. Energies for the first excited state are given in brackets.

	E_A	ΔE
$H_2 \rightarrow 2H$	1.16 (0.75)	−0.04 (-0.25)
$CO_2 \rightarrow CO + O$	1.66 (1.64)	−0.67 (-0.15)
$CO_2 + H \rightarrow$ *t-HOCO*	1.71 (1.67)	0.47 (1.67)
c-HOCO $\rightarrow CO + OH$	0.40 (0.27)	−0.41 (-0.39)
$H_2O \rightarrow OH + H$	0.14 (0.01)	−1.46 (-1.60)
c-HOCO $\rightarrow$ *t-HOCO*	0.68 (0.00)	−0.06 (-1.02)

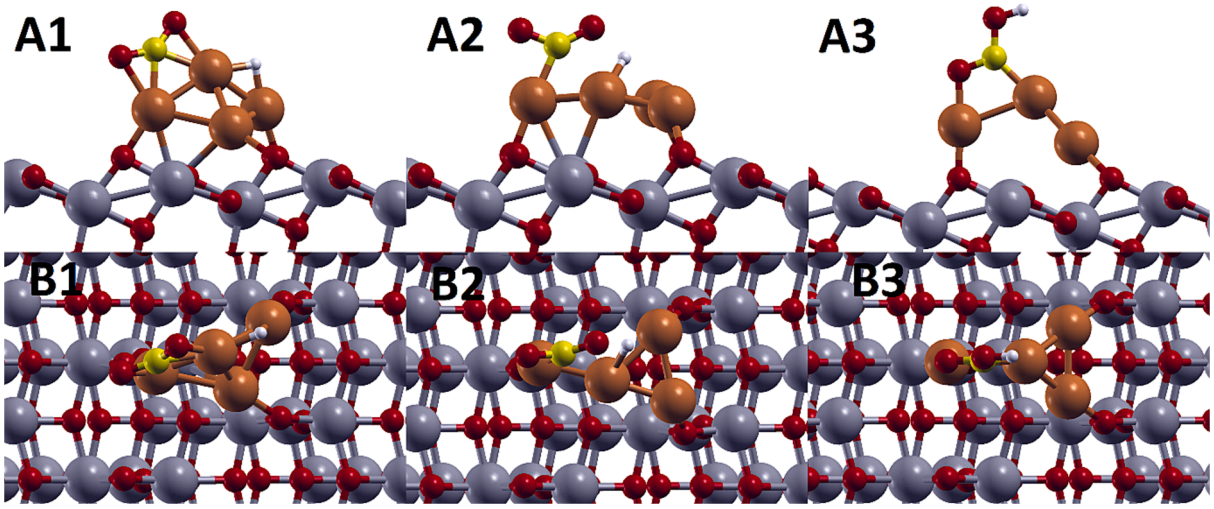

Fig. 4. CO_2 hydrogenation over Cu/anatase(1 0 1) surface, where 1 is the initial, 2 saddle, 3 final structure, and A denotes side, and B side view.

Table 9
Adsorption energies [in eV] over the Cu/rutile (1 1 0) surface.

	E_{ads}
CO_2	−0.28
CO	−0.45
c-HOCO	−2.89
H_2	−0.21
H_2O	−0.13

In Table 10, we see that H_2 dissociation has a low barrier with only 0.35 eV and is highly exothermic at −1.62 eV. Similarly, H_2O dissociation is likely with a barrier 0.15 eV and exothermic. CO_2 can therefore be either hydrogenated to form HOCO or dissociate (Fig. 5). The latter pathway is preferred with a barrier of 1.05 eV compared to 1.63 eV. The direct dissociation has the most favorable E_A of all the studied surfaces, whereas direct hydrogenation (1.63 eV) is inhibited compared to the pristine rutile (1 1 0) surface (1.23 eV). A high E_A of HOCO dissociation (1.29 eV) suggests it might react further to produce methanol or methane. The initial, saddle and final structures are shown in Fig. S6.

Lastly, excited states were included. Again, dissociation of H_2 is spontaneous and the barrier for H_2O dissociation is also very low. Furthermore the direct dissociation of CO_2 is significantly more likely as the barrier is lowered from 1.04 to 0.68 eV. On the other hand, the hydrogenation of CO_2 to form HOCO has E_A of 1.58 eV and is virtually unaffected. This strongly hints that the direct dissociation of CO_2 is the dominant reaction pathway. Due to low adsorption energy of CO (-0.45 eV), it is also likely to be the major product. The barrier for the dissociation of HOCO is slightly lowered relative to the ground state.

The calculated band gap of Cu_4/rutile (1 1 0) was calculated at 0.95 eV, which is smaller than in the pristine rutile (1 1 0) surface and attributed to the orbital overlap of Cu atoms with the TiO_2 surface.

Table 10
Activation barriers and reaction energies [eV] for ground-state CO_2 reduction over Cu_4-rutile (1 1 0) surface. Energies for the first excited state are given in brackets.

	E_A	ΔE
$H_2 \rightarrow 2H$	0.35 (0.00)	−1.62 (-1.65)
$CO_2 \rightarrow CO + O$	1.05 (0.68)	0.87 (0.68)
$CO_2 + H \rightarrow$ *c-HOCO*	1.63 (1.56)	1.00 (1.15)
t-HOCO $\rightarrow CO + OH$	1.29 (1.14)	0.17 (0.19)
$H_2O \rightarrow OH + H$	0.15 (0.00)	−1.78 (-1.75)
c-HOCO $\rightarrow$ *t-HOCO*	1.47 (1.26)	−0.05 (-0.06)

Comparing the band gaps of the studied surfaces, we observe that the pristine anatase (1 0 1) surface has the highest band gap at 2.36 eV, followed by pristine rutile (1 1 0), Cu_4-rutile (1 1 0) and Cu_4-anatase (1 0 1) with band gaps of 1.21, 0.95 and 0.35 eV respectively. Nevertheless we would like to emphasize that these are attributed to the surface doping of Cu clusters on the surface, which hybridize with the TiO_2 surface and artificially lower the band gap. The band gap of the TiO_2 system elsewhere is larger, closer to the pristine TiO_2 surface studied. Thus we conclude that higher energy photo-excitations are also possible.

Studying the effect of photoexcitation, a decrease in the activation barriers is observed in our model. In the excited state, the barrier for CO_2 hydrogenation is 2–11 % lower for the investigated TiO_2 structures. This values are dependent on the functional used, the catalyst surface etc. but show a general trend and explain why photocatalysis is a viable approach for CO_2 reduction.

3.2. Microkinetic model

Microkinetic modelling is a useful tool to further analyze the first-principles results. In this section, we describe a microkinetic model, which was adapted for each surface. While the reaction mechanism was kept as simple as possible to be able to evaluate individual contributions, microkinetics serves an important role. First, it proves that the calculated reaction parameters *can* produce the desire products and, secondly, that allows us to evaluate the *trends* while varying temperatures and reactant ratios.

We varied the ratio of CO_2 and H_2O, where CO_2 was reduced to CO and H_2O was used as a hydrogen source upon irradiation. Thus, CO is produced but water splitting, which yields H_2, is a possible undesired side reaction.

As discussed in previous sections, the Cu (1 1 1) surface is metallic and cannot operate in the photoexcited regime. Therefore, we only used the parameters for the ground state as an input. On TiO_2, we selected the most thermodynamically stable surface facets of rutile and anatase, namely (1 1 0) and (1 0 1), respectively. Firstly, we input the DFT-calculated parameters for the ground state into the microkinetic model. The results indicated that the pristine rutile and anatase were unable to efficiently activate and reduce CO_2 in the ground state at mild conditions, which is consistent with prior literature reports [65]. Although the inclusion of excited states significantly reduces the activation barriers, they remain too high for the catalysts to be active for photo-reducing CO_2. Additionally, it is well-established that pristine TiO_2 experiences high recombination rates [66,67], which further impedes its activity. However, this is not explicitly taken into account in

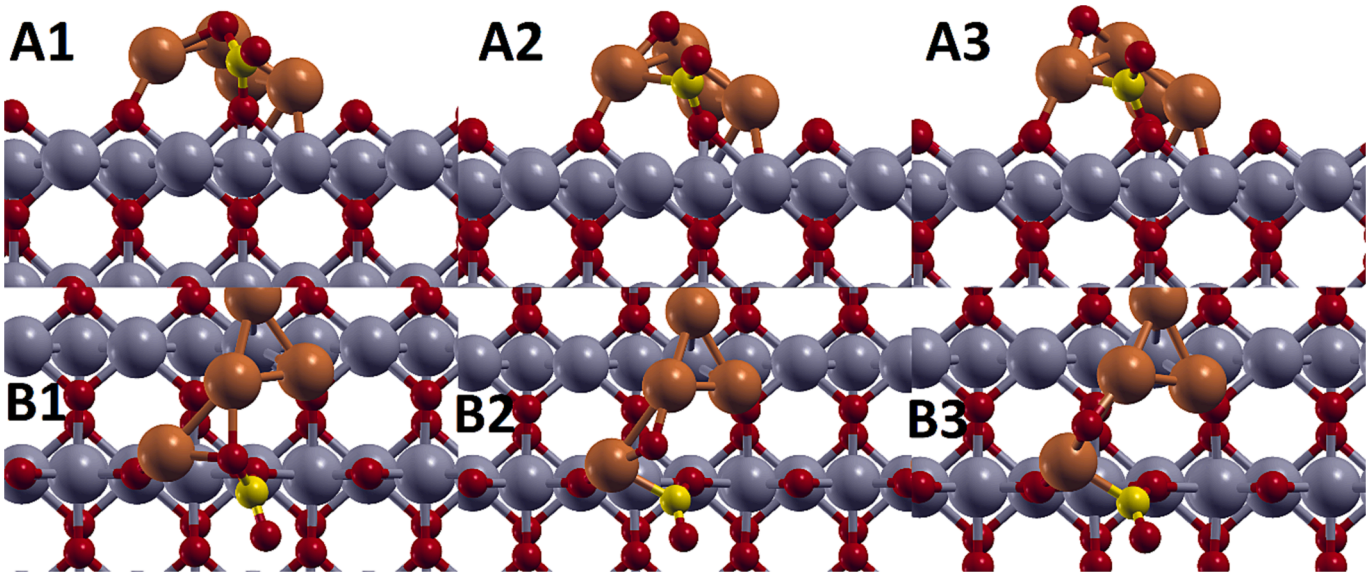

Fig. 5. CO_2 dissociation over Cu/Rutile (1 1 0) surface, where 1 is the initial, 2 saddle, 3 final structure, and A denotes side, and B side view.

the model.

Based on the DFT findings, we can infer that Cu (1 1 1) exhibits a higher activity for CO_2 reduction than TiO_2 in the ground state. TiO_2 is only useful for water splitting. Thus, we limit our microkinetic simulations to the two Cu_4/TiO_2 scenarios.

3.2.1. Cu/Rutile (1 1 0)

No significant formation of CO was observed on the pristine surfaces (Cu (1 1 1), rutile and anatase), indicating their inability to effectively photoreduce CO_2 under mild reaction conditions. On Cu/rutile (1 1 0), we varied the feed ratio CO_2:H_2O namely from 1:20 to 10:1, while keeping the other reaction parameters constant. The results indicate that CO_2 hydrogenation is not favorable and no COOH or H_2 is formed, whereas CO production is highly dependent on the feed composition. We found that the optimal CO_2:H_2O feed ratio for CO production is 4:1. The temporal evolution is shown in Fig. 6.

We see that H_2O adsorbs and immediately dissociates to create OH and O, while CO_2 only adsorbs to the surface. Then, the dissociation of CO_2 to form CO and O starts, with the hydrogen produced from water splitting being utilized to generate OH. The dotted green line indicates that CO desorbs from the surface. Our findings are consistent with the study conducted by Liu et al. [68], where they investigated the impact of Cu doping on TiO_2 for the photocatalytic reduction of CO_2 to CO and methane. They reported CO as the primary product, and a small amount of CH_4 was also generated. Li et al. [69] found that Cu doped TiO_2 catalysts over silica support produced mainly CO, while small amounts of methane were also produced.

3.2.2. Cu/Anatase (1 0 1)

Contrary to the Cu/rutile (1 1 0) surface where CO was the major product, we observed H_2 to be the predominant product in this case. This is consistent with the findings from the analysis of DFT data, where

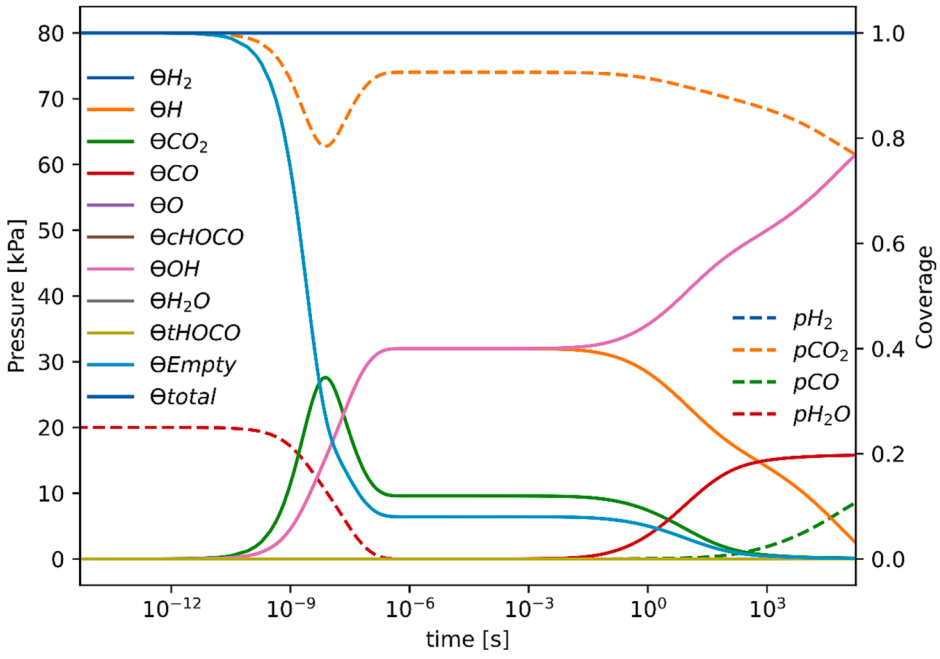

Fig. 6. The temporal evolution in the CO_2 photo-reduction on the Cu/rutile (1 1 0) surface with the species in the excited state.

water splitting was found to be more favourable.

As shown in Figs. 7, H_2O initially adsorbs and dissociates on the surface, while CO_2 adsorbs briefly and desorbs due to a weaker adsorption energy. This is attributed to the stronger adsorption energies of OH and H relative to CO_2. The adsorbed H then reacts to form H_2, which subsequently desorbs and leaves more active sites available, facilitating further water splitting. These results are consistent with the experimental findings of Ola et al. [70], who investigated the use of Cu-doped TiO_2 monoliths for CO_2 photoreduction. In their studies, the wt% of anatase was 90 % or higher in all cases, indicating that it governs the reaction. They found that H_2 was the predominant product, with other products such as methanol, ethanol, and acetaldehyde detected in smaller quantities.

Lastly, we tested the effect of varying feed composition. Fig. 8 displays the calculated turnover frequencies (TOF) for CO production on Cu/rutile (1 1 0) and H_2 production over Cu/anatase (1 0 1). The results indicate that the maximum TOF for the ground state is about 10^4 times smaller than that for the excited state. Fig. 8 further shows that the TOF is highly dependent on the CO_2 to H_2O ratio. The partial pressure of H_2O was incremented in steps of 5 kPa, while the sum of $p(H_2O)$ and $p(CO_2)$ remained constant at 1 bar.

At 20 % H_2O, the maximum TOF for Cu/rutile (1 1 0) is observed. This can be attributed to the optimal amount of hydrogen present to hydrogenate the produced oxygen from CO_2 dissociation, which facilitates CO desorption from the surface due to stronger OH adsorption. However, a larger H_2O ratio produces excessive OH from water splitting, which poisons the catalyst. Cu/anatase (1 0 1) reaches its maximum TOF at $p(H_2O)$ of 30 kPa and the TOF remains unchanged despite an increase in the partial pressure of H_2O. This can be attributed to the poisoning of the surface with OH group, which does not speed up the reaction at higher pressures.

Our results indicate that Cu/rutile (1 1 0) favors CO production, while Cu/anatase (1 0 1) primarily generates H_2, which agrees with prior research. Altering the reaction feed has been demonstrated to have a substantial effect on product distribution.

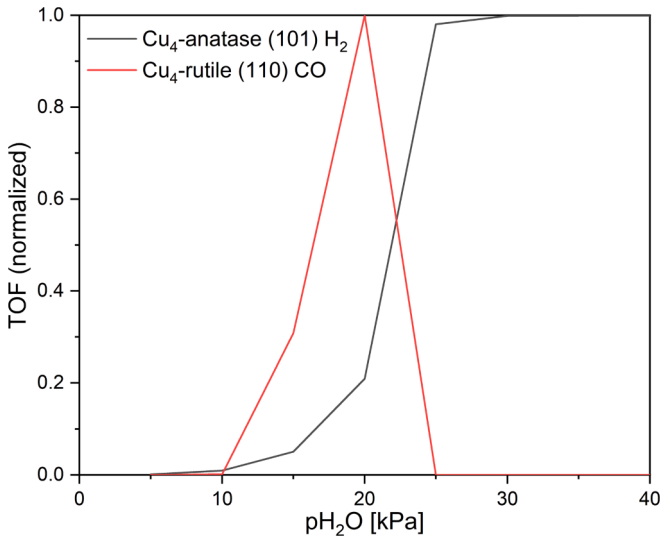

Fig. 8. Turnover frequency (TOF) for CO (red) and H_2 (black) production over Cu/rutile (1 1 0) and Cu_4-anatase (1 0 1) respectively. (For interpretation of the references to color in this figure legend, the reader is referred to the web version of this article.)

4. Conclusion

The photocatalytic reduction of CO_2 has recently generated increased interest from academia as well as the industry due to its prospects in tackling the climate crisis. Although there have been many reports on CO_2 photoreduction on different catalysts and their modifications, most of the work is experimental. Most of the theoretical studies do not explicitly incorporate excited states, meaning that the process is approximated as thermocatalytic rather than photocatalytic.

We explicitly considered the excited states during CO_2 photoreduction with the ΔSCF method. Due to Kasha's rule, we only considered the

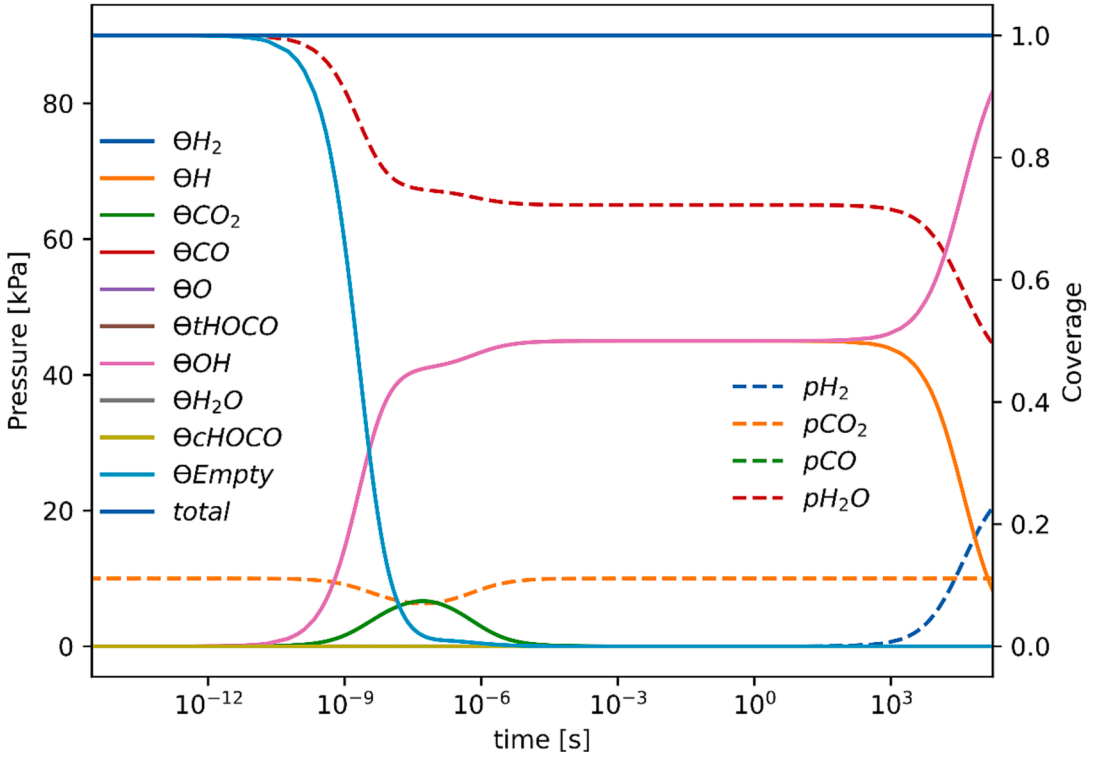

Fig. 7. The temporal evolution in the CO_2 photo-reduction on the Cu/anatase (1 0 1) surface with the species in the excited state.

first excited state. For Cu (1 1 1), no differences were observed on account of its metallicity. Consequently, the rutile and anatase crystal phases of TiO_2 were chosen as benchmark and the most researched photocatalysts in the literature. We showed that photo-excitation has a significant impact on the activation barriers, which can be significantly reduced. Nevertheless the pristine facets are rather inactive for the CO_2 reduction. Lastly, we deposited four Cu atoms on the rutile (1 1 0) and anatase (1 0 1) surfaces as a computationally tractable model of the Cu/TiO_2 formulation.

On Cu (1 1 1), surface we can expect the direct dissociation of CO_2 to form CO and hydrogenation of CO_2 under *thermocatalytic* conditions. The relatively high CO adsorption energy might hints that it is unlikely to desorb and indeed Cu is a well-known catalyst for the formation of C_{2+} products. There is little change in its photocatalytic performance due to the overlapping valence and conduction bands (no band gap).

On the other hand, pristine anatase (1 0 1) exhibits a high band gap of 2.36 eV. The ground state calculations reveal CO_2 would be reduced through direct hydrogenation, but this is unlikely due to a high activation barrier. Inclusion of the excited states significantly reduces the barriers. CO adsorption strength is rather weak, which is also the case for pristine rutile (1 1 0) surface. A direct CO_2 dissociation is again impossible due to unfavourable thermodynamics. The most likely reaction pathway is the direct hydrogenation to HOCO, which then likely reacts further towards methane or methanol. The reaction rates in all cases are negligible.

Finally, we deposited four Cu atoms on rutile and anatase. Contrary to pristine anatase (1 0 1) surface, the Cu/anatase (1 0 1) surface has much lower activation energies in the ground state, where results suggest that hydrogenation and dissociation of CO_2 are almost equally likely to happen. After the formation, HOCO can then react further or dissociate to CO and OH. Inclusion of excited states furthermore reveals that the activation barriers are further lowered. In the case of Cu/rutile (1 1 0), it was found that in the ground state the direct dissociation of CO_2 is likely the predominant pathway, whereas hydrogenation has a higher barrier. Due to low adsorption energies of CO, it is also likely to be the major product. The inclusion of excited states even further lowers the E_A.

It should be noted that Cu-clusters on a TiO_2 surface introduce cluster states in the band gap, which themselves do not significantly influence it as shown in Fig. 2. This is expected as cluster states do not have a sufficient cross section to influence an optical measurement but they can function as recombination sites. Consequently, the photo-excited electrons have substantial energy inside TiO2 but the overall efficiency of the system can be lowered by the recombination sites.

Subsequently, a microkinetic model was constructed to investigate the evolution of the participating species on all five photocatalytic surfaces. In the ground state, CO_2 reduction did not proceed at the mild reaction conditions of 1 bar and 298 K, which was expected. However, accounting for the excited states revealed that Cu/rutile (1 1 0) and Cu/anatase (1 0 1) surfaces are active. The former was active for water splitting, forming predominantely H_2, whereas Cu/anatase (1 0 1) favored the production of CO. The results were found to agree with other experimental studies, reinforcing the importance of including excited states in DFT calculations and subsequent macro-scale models.

In this study, we have included the excited states in modelling the reaction mechanism for photocatalytic CO_2 reduction to CO as a model reaction. We have shown that this significantly changes the reaction barriers, invalidating the common approach of including them only when studying the catalyst properties. Despite simplifications and approximations, we have obtained results that match existing experimental data. To the best of our knowledge, no other research has implemented excited states on such a comprehensive level, leading to the development of ground state versus excited state microkinetic models. This approach has provided valuable insights into the significance of incorporating excited states. The obtained results demonstrate good agreement with experimental photoexcited studies, showcasing the applicability of this study beyond CO_2 photo-reduction to other desired species. Researchers can leverage these findings for a wide range of applications.

CRediT authorship contribution statement

Žan Kovačič: Conceptualization, Data curation, Formal analysis, Investigation, Methodology, Visualization, Writing – original draft. **Blaž Likozar:** Funding acquisition, Project administration, Writing – review & editing. **Matej Huš:** Conceptualization, Investigation, Supervision, Writing – review & editing.

Declaration of competing interest

The authors declare that they have no known competing financial interests or personal relationships that could have appeared to influence the work reported in this paper.

Data availability

Data will be made available on request.

Acknowledgements

The authors acknowledge the Slovenian Research Agency (ARRS) for funding this research. B. L. appreciates the core funding P2-0152 and project funding J7-4638, J2-4441 and N2-0310. M. H. is supported by the core funding P2-0421, project funding J1-3028 and infrastructure funding I0-0039. Ž. K. is funded by the project N1-0303. Financial support by the European Commission through Horizon Europe funding (CATART project, Grant Agreement 101046836) is appreciated.

Appendix A. Supplementary data

Supplementary data to this article can be found online at https://doi.org/10.1016/j.cej.2024.149894.

References

[1] A.J. Haider, Z.N. Jameel, I.H.M. Al-Hussaini, Review on: titanium dioxide applications, Energy Procedia 157 (2019) 17–29, https://doi.org/10.1016/j.egypro.2018.11.159.
[2] S. Mo, W.Y. Ching, Electronic and optical properties of three phases of titanium dioxide: rutile, anatase, and brookite, Phys. Rev. B 51 (1995) 13023–13032.
[3] X. Wang, F. Wang, Y. Sang, H. Liu, Full-Spectrum solar-light-activated photocatalysts for light – chemical energy conversion, Adv. Energy Mater. 7 (2017) 1700473, https://doi.org/10.1002/aenm.201700473.
[4] Ş. Neaţu, J.A. Maciá-Agulló, H. Garcia, Solar light photocatalytic CO2 reduction: general considerations and selected bench-mark photocatalysts, Int. J. Mol. Sci. 15 (2014) 5246–5262, https://doi.org/10.3390/ijms15045246.
[5] A.K. Singh, K. Mathew, H.L. Zhuang, R.G. Hennig, Computational screening of 2D materials for photocatalysis, J. Phys. Chem. Lett. 6 (2015) 1087–1098, https://doi.org/10.1021/jz502646d.
[6] M. Tahir, N.A.S. Amin, Indium-doped TiO2 nanoparticles for photocatalytic CO2 reduction with H2O vapors to CH4, Appl. Catal. B Environ. 162 (2015) 98–109, https://doi.org/10.1016/j.apcatb.2014.06.037.
[7] S.B. Patil, P.S. Basavarajappa, N. Ganganagappa, M.S. Jyothi, A.V. Raghu, K. R. Reddy, Recent advances in non-metals-doped TiO2 nanostructured photocatalysts for visible-light driven hydrogen production, CO2 reduction and air purification, Int. J. Hydrogen Energy 44 (2019) 13022–13039, https://doi.org/10.1016/j.ijhydene.2019.03.164.
[8] X. Li, J. Yu, M. Jaroniec, X. Chen, Cocatalysts for selective photoreduction of CO 2 into solar fuels, Chem. Rev. 119 (2019) 3962–4179, https://doi.org/10.1021/acs.chemrev.8b00400.
[9] M. Moradi, F. Khorasheh, A. Larimi, Pt nanoparticles decorated bi-doped TiO2 as an efficient photocatalyst for CO2 photo-reduction into CH4, Sol. Energy 211 (2020) 100–110, https://doi.org/10.1016/j.solener.2020.09.054.
[10] A.T. Montoya, E.G. Gillan, Enhanced photocatalytic hydrogen evolution from transition-metal surface-modified TiO2, ACS Omega 3 (2018) 2947–2955, https://doi.org/10.1021/acsomega.7b02021.
[11] T.T.Y. Tan, C.K. Yip, D. Beydoun, R. Amal, Effects of nano-ag particles loading on TiO 2 photocatalytic reduction of selenate ions, Chem. Eng. J. 95 (2003) 179–186, https://doi.org/10.1016/S1385-8947(03)00103-7.

[12] J. Li, M. Zhang, Z. Guan, Q. Li, C. He, J. Yang, Synergistic effect of surface and bulk single-electron-trapped oxygen vacancy of TiO2 in the photocatalytic reduction of CO2, Appl. Catal. B Environ. 206 (2017) 300–307, https://doi.org/10.1016/j.apcatb.2017.01.025.

[13] J. Low, B. Dai, T. Tong, C. Jiang, J. Yu, In situ irradiated X-ray photoelectron spectroscopy investigation on a direct Z-scheme TiO2/CdS composite film photocatalyst, Adv. Mater. 31 (2019) 1802981, https://doi.org/10.1002/adma.201802981.

[14] G. Yang, D. Chen, H. Ding, J. Feng, J.Z. Zhang, Y. Zhu, S. Hamid, D.W. Bahnemann, Well-designed 3D ZnIn2S4 nanosheets/TiO2 nanobelts as direct Z-scheme photocatalysts for CO2 photoreduction into renewable hydrocarbon fuel with high efficiency, Appl. Catal. B Environ. 219 (2017) 611–618, https://doi.org/10.1016/j.apcatb.2017.08.016.

[15] K. Ozawa, M. Emori, S. Yamamoto, R. Yukawa, S. Yamamoto, R. Hobara, K. Fujikawa, H. Sakama, I. Matsuda, Electron-hole recombination time at TiO2 single-crystal surfaces: influence of surface band bending, J. Phys. Chem. Lett. 5 (2014) 1953–1957, https://doi.org/10.1021/jz500770c.

[16] J. Zhuang, W. Dai, Q. Tian, Z. Li, L. Xie, J. Wang, P. Liu, X. Shi, D. Wang, Photocatalytic degradation of RhB over TiO2 bilayer films: effect of defects and their location, Langmuir 26 (2010) 9686–9694, https://doi.org/10.1021/la100302m.

[17] J. Wang, D.N. Tafen, J.P. Lewis, Z. Hong, A. Manivannan, M. Zhi, M. Li, N. Wu, Origin of photocatalytic activity of nitrogen-doped TiO2 nanobelts, J. Am. Chem. Soc. 131 (2009) 12290–12297, https://doi.org/10.1021/ja903781h.

[18] A. Yang, J. Luo, Z. Xie, Q. Chen, Photocatalytic activity of V2O5/ZnV2O6 catalysts and its origin: insights into enhanced photocatalytic mechanisms via DFT study, Appl. Surf. Sci. 599 (2022) 153894, https://doi.org/10.1016/j.apsusc.2022.153894.

[19] Y. Wang, Y. Tian, L. Yan, Z. Su, DFT study on sulfur-doped g - C 3 N 4 nanosheets as a photocatalyst for CO 2 reduction reaction, J. Phys. Chem. C 122 (2018) 7712–7719, https://doi.org/10.1021/acs.jpcc.8b00098.

[20] K. Wang, J. Fu, Y. Zheng, Insights into photocatalytic CO2 reduction on C3N4: strategy of simultaneous B, K CO-doping and enhancement by N vacancies, Appl. Catal. B Environ. 254 (2019) 270–282, https://doi.org/10.1016/j.apcatb.2019.05.002.

[21] Y. Ji, Y. Luo, New mechanism for photocatalytic reduction of CO2 on the anatase TiO2(101) surface: the essential role of oxygen vacancy, J. Am. Chem. Soc. 138 (2016) 15896–15902, https://doi.org/10.1021/jacs.6b05695.

[22] P.T. Van Duijnen, H.D. De Gier, R. Broer, R.W.A. Havenith, The behaviour of charge distributions in dielectric media, Chem. Phys. Lett. 615 (2014) 83–88, https://doi.org/10.1016/j.cplett.2014.10.003.

[23] L.F. Li, Y.F. Li, Z.P. Liu, CO2 photoreduction via quantum tunneling: thin TiO2-coated GaP with coherent Interface to achieve electron tunneling, ACS Catal. 9 (2019) 5668–5678, https://doi.org/10.1021/acscatal.9b01645.

[24] K.K. Ghuman, L.B. Hoch, P. Szymanski, J.Y.Y. Loh, N.P. Kherani, M.A. El-Sayed, G. A. Ozin, C.V. Singh, Photoexcited surface frustrated Lewis pairs for heterogeneous photocatalytic CO2 reduction, J. Am. Chem. Soc. 138 (2016) 1206–1214, https://doi.org/10.1021/jacs.5b10179.

[25] T. Le, Y. Shao, B. Wang, Plasmon-induced CO2Conversion on Al@Cu2O: a DFT study, J. Phys. Chem. C 125 (2021) 6108–6115, https://doi.org/10.1021/acs.jpcc.0c10957.

[26] A. Hellman, B. Razaznejad, B.I. Lundqvist, Potential-energy surfaces for excited states in extended systems, J. Chem. Phys. 120 (2004) 4593–4602, https://doi.org/10.1063/1.1645787.

[27] M. Kasha, Characterization of electronic transitions in complex molecules, Discuss. Faraday Soc. 9 (1950) 14–19, https://doi.org/10.1039/DF9500900014.

[28] G. Krese, J. Furthmüller, Efficient iterative schemes for ab initio total-energy calculations using a plane-wave basis set, Phys. Rev. B 54 (1996) 11169–11186, https://doi.org/10.1063/1.2104507.

[29] J.P. Perdew, K. Burke, M. Ernzerhof, Generalized gradient approximation made simple, Phys. Rev. Lett. 77 (1996) 3865–3868, https://doi.org/10.1103/PhysRevLett.77.3865.

[30] P.E. Blöchl, Projector augmented-wave method, Phys. Rev. B 50 (1994) 17953–17979.

[31] J. Hubbard, P.R.S.L. A, Electron correlations in narrow energy bands, Proc. R. Soc. London. Ser. A. Math. Phys. Sci. 276 (1963) 238–257. 10.1098/rspa.1963.0204.

[32] K. Chen, C. Chen, X. Ren, A. Alsaedi, T. Hayat, Interaction mechanism between different facet TiO 2 and U (VI): experimental and density-functional theory investigation, Chem. Eng. J. 359 (2019) 944–954, https://doi.org/10.1016/j.cej.2018.11.092.

[33] X. Lin, Y. Yoon, N.G. Petrik, Z. Li, Z. Wang, V. Glezakou, B.D. Kay, I. Lyubinetsky, G.A. Kimmel, R. Rousseau, Z. Dohna, Structure and dynamics of CO2 on rutile TiO2 (110) -1 × 1, J. Phys. Chem. C 116 (2012) 26322–26334, https://doi.org/10.1021/jp308061j.

[34] S.L. Dudarev, G.A. Botton, S.Y. Savrasov, C.J. Humphreys, A.P. Sutton, Electron-energy-loss spectra and the structural stability of nickel oxide: an LSDA+U study, Phys. Rev. B 57 (1998) 1505–1509.

[35] S. Grimme, J. Antony, S. Ehrlich, H. Krieg, parametrization of density functional dispersion correction (DFT-D) for the 94 elements H-pu dispersion correction „ DFT-D for the 94 elements H-pu, J. Chem. Phys. 132 (2010) 154104, https://doi.org/10.1063/1.3382344.

[36] L. Bengtsson, Dipole correction for surface supercell calculations, Phys. Rev. B - Condens. Matter Mater. Phys. 59 (1999) 12301–12304, https://doi.org/10.1103/physrevb.61.16921.

[37] H.J. Monkhorst, J.D. Pack, Special points for brillouin-zone integrations, Phys. Rev. B 13 (1976) 5188–5192, https://doi.org/10.1103/PhysRevB.16.1748.

[38] G. Henkelman, B.P. Uberuaga, H. Jónsson, Climbing image nudged elastic band method for finding saddle points and minimum energy paths, J. Chem. Phys. 113 (2000) 9901–9904, https://doi.org/10.1063/1.1329672.

[39] A. Heyden, A.T. Bell, F.J. Keil, Efficient methods for finding transition states in chemical reactions: comparison of improved dimer method and partitioned rational function optimization method, J. Chem. Phys. 123 (2005) 224101, https://doi.org/10.1063/1.2104507.

[40] R.J. Baxter, P. Hu, Insight into why the langmuir-hinshelwood mechanism is generally preferred, J. Chem. Phys. 116 (2002) 4379–4381, https://doi.org/10.1063/1.1458938.

[41] A. Bjelajac, D. Kopač, A. Fecant, E. Tavernier, R. Petrović, B. Likozar, D. Janaćković, Micro-kinetic modelling of photocatalytic CO2 reduction over undoped and N-doped TiO2, catal, Sci. Technol. 10 (2020) 1688–1698, https://doi.org/10.1039/c9cy02443c.

[42] L. Skubic, D. Kopač, B. Likozar, M. Huš, Microkinetic modelling of heterogeneous catalysis revisited: adsorption energies can triumph over activation barriers, Appl. Surf. Sci. 601 (2022) 154135, https://doi.org/10.1016/j.apsusc.2022.154135.

[43] H. Tang, H. Berger, P.E. Schmid, F. Levy, Photoluminescence in TiO2 anatase single crystals, Solid State Commun. 87 (1993) 647–850, https://doi.org/10.1016/0038-1098(93)90427-O.

[44] Á. Morales-García, R. Valero, F. Illas, An empirical, yet practical way to predict the band gap in solids by using density functional band structure calculations, J. Phys. Chem. C 121 (2017) 18862–18866, https://doi.org/10.1021/acs.jpcc.7b07421.

[45] Y. Zhen Fang, X. Jin Kong, D. Ting Wang, S. Xin Cui, J. Hai Liu, Role of dopant ga in tuning the band gap of rutile TiO2 from first principles, chinese, J. Phys. 56 (2018) 1370–1377, https://doi.org/10.1016/j.cjph.2018.04.011.

[46] R. Zhang, J. Zhao, Y. Yang, Z. Lu, W. Shi, Understanding electronic and optical properties of la and mn co-doped anatase TiO2, Comput. Condens. Matter 6 (2016) 5–17, https://doi.org/10.1016/j.cocom.2016.03.001.

[47] J. Jia, H. Wang, Z. Lu, P.G. O'Brien, M. Ghoussoub, P. Duchesne, Z. Zheng, P. Li, Q. Qiao, L. Wang, A. Gu, A.A. Jelle, Y. Dong, Q. Wang, K.K. Ghuman, T. Wood, C. Qian, Y. Shao, C. Qiu, M. Ye, Y. Zhu, Z.H. Lu, P. Zhang, A.S. Helmy, C.V. Singh, N.P. Kherani, D.D. Perovic, G.A. Ozin, Photothermal catalyst engineering: hydrogenation of gaseous CO 2 with high activity and tailored selectivity, Adv. Sci. 4 (2017) 1700252, https://doi.org/10.1002/advs.201700252.

[48] B. Yu, Y. Zhou, P. Li, W. Tu, P. Li, L. Tang, J. Ye, Z. Zou, Photocatalytic reduction of CO2 over Ag/TiO2 nanocomposites prepared with a simple and rapid silver mirror method, Nanoscale 8 (2016) 11870–11874, https://doi.org/10.1039/c6nr02547a.

[49] L.C. Grabow, M. Mavrikakis, Mechanism of methanol synthesis on cu through CO2 and CO hydrogenation, ACS Catal. 1 (2011) 365–384, https://doi.org/10.1021/cs200055d.

[50] M.H.N. Assadi, D.A.H. Hanaor, The effects of copper doping on photocatalytic activity at (101) planes of anatase TiO2: a theoretical study, Appl. Surf. Sci. 387 (2016) 682–689, https://doi.org/10.1016/j.apsusc.2016.06.178.

[51] D.C. Sorescu, W.A. Al-Saidi, K.D. Jordan, CO2 adsorption on TiO2(101) anatase: a dispersion-corrected density functional theory study, J. Chem. Phys. 135 (2011) 124701, https://doi.org/10.1063/1.3638181.

[52] R. Wanbayor, P. Deák, T. Frauenheim, V. Ruangpornvisuti, First principles theoretical study of the hole-assisted conversion of CO to CO2 on the anatase TiO2 (101) surface, J. Chem. Phys. 134 (2011) 104701, https://doi.org/10.1063/1.3562366.

[53] Z. Wang, X. Wang, H. Wang, X. Chen, W. Dai, X. Fu, The mechanism of photodriven oxidation of CO over anatase and rutile TiO2 investigated from the hydrogen adsorption behavior, Appl. Catal. B Environ. 277 (2020) 119169, https://doi.org/10.1016/j.apcatb.2020.119169.

[54] A. Vittadini, A. Selloni, F.P. Rotzinger, M. Grätzel, Structure and energetics of water adsorbed at TiO2 anatase (101) and (001) surfaces, Phys. Rev. Lett. 81 (1998) 2954–2957, https://doi.org/10.1103/PhysRevLett.81.2954.

[55] C.T. Yang, B.C. Wood, V.R. Bhethanabotla, B. Joseph, CO2 adsorption on anatase TiO2 (101) surfaces in the presence of subnanometer Ag/Pt clusters: implications for CO2 photoreduction, J. Phys. Chem. C 118 (2014) 26236–26248, https://doi.org/10.1021/jp509219n.

[56] H. He, P. Zapol, L.A. Curtiss, Computational screening of dopants for photocatalytic two-electron reduction of CO 2 on anatase (101) surfaces, Energ. Environ. Sci. 5 (2012) 6196–6205, https://doi.org/10.1039/c2ee02665a.

[57] P. Verma, D.G. Truhlar, Does DFT+U mimic hybrid density functionals? Theor. Chem. Acc. 135 (2016) 1–15, https://doi.org/10.1007/s00214-016-1927-4.

[58] D.C. Sorescu, J. Lee, W.A. Al-saidi, K.D. Jordan, CO2 adsorption on TiO2 (110) rutile : insight from dispersion-corrected density functional theory calculations and scanning tunneling, J. Chem. Phys. 134 (2011) 104707, https://doi.org/10.1063/1.3561300.

[59] L.A. Harris, A.A. Quong, Molecular chemisorption as the theoretically preferred pathway for water adsorption on ideal rutile TiO2(110), Phys. Rev. Lett. 93 (2004) 086105, https://doi.org/10.1103/PhysRevLett.93.086105.

[60] A. Lyalin, T. Taketsugu, A computational investigation of H2 adsorption and dissociation on au nanoparticles supported on TiO2 surface, Faraday Discuss. 152 (2011) 185–201, https://doi.org/10.1039/c1fd00013f.

[61] M. Reticcioli, I. Sokolović, M. Schmid, U. Diebold, M. Setvin, C. Franchini, Interplay between adsorbates and polarons: CO on rutile TiO2 (110), Phys. Rev. Lett. 122 (2019) 016805, https://doi.org/10.1103/PhysRevLett.122.016805.

[62] A. Bayani, J. Gebhardt, C. Elsässer, Electronic bulk and surface properties of titanium dioxide studied by DFT-1/2, Langmuir 39 (2023) 14922–14934, https://doi.org/10.1021/acs.langmuir.3c01698.

[63] N. Singhal, A. Ali, A. Vorontsov, C. Pendem, U. Kumar, Efficient approach for simultaneous CO and H2 production via photoreduction of CO2 with water over

copper nanoparticles loaded TiO2, Appl. Catal. A 523 (2016) 107–117, https://doi.org/10.1016/j.apcata.2016.05.027.
[64] I.H. Tseng, J.C.S. Wu, H.Y. Chou, Effects of sol-gel procedures on the photocatalysis of Cu/TiO2 in CO2 photoreduction, J. Catal. 221 (2004) 432–440, https://doi.org/10.1016/j.jcat.2003.09.002.
[65] Y. Cao, Q. Li, C. Li, J. Li, J. Yang, Surface heterojunction between (001) and (101) facets of ultrafine anatase TiO2 nanocrystals for highly efficient photoreduction CO2 to CH4, Appl. Catal. B Environ. 198 (2016) 378–388, https://doi.org/10.1016/j.apcatb.2016.05.071.
[66] A. Meng, J. Zhang, D. Xu, B. Cheng, J. Yu, Enhanced photocatalytic H2-production activity of anatase TiO2 nanosheet by selectively depositing dual-cocatalysts on (101) and (001) facets, Appl. Catal. B Environ. 198 (2016) 286–294, https://doi.org/10.1016/j.apcatb.2016.05.074.
[67] R. Qian, H. Zong, J. Schneider, G. Zhou, T. Zhao, Y. Li, J. Yang, D.W. Bahnemann, J.H. Pan, Charge carrier trapping, recombination and transfer during TiO2 photocatalysis: an overview, Catal. Today 335 (2019) 78–90, https://doi.org/10.1016/j.cattod.2018.10.053.
[68] L. Liu, F. Gao, H. Zhao, Y. Li, Tailoring cu valence and oxygen vacancy in Cu/TiO2 catalysts for enhanced CO2 photoreduction efficiency, Appl. Catal. B Environ. 134–135 (2013) 349–358, https://doi.org/10.1016/j.apcatb.2013.01.040.
[69] Y. Li, W.N. Wang, Z. Zhan, M.H. Woo, C.Y. Wu, P. Biswas, Photocatalytic reduction of CO2 with H2O on mesoporous silica supported Cu/TiO2 catalysts, Appl. Catal. B Environ. 100 (2010) 386–392, https://doi.org/10.1016/j.apcatb.2010.08.015.
[70] O. Ola, M. Mercedes Maroto-Valer, Copper based TiO2 honeycomb monoliths for CO2 photoreduction, Cat. Sci. Technol. 4 (2014) 1631–1637, https://doi.org/10.1039/c3cy00991b.